

## Indirect structural health monitoring of a simplified laboratory-scale bridge model

Fernando Cerda<sup>\*1</sup>, Siheng Chen<sup>2</sup>, Jacobo Bielak<sup>3</sup>, James H. Garrett<sup>3</sup>,  
Piervincenzo Rizzo<sup>5</sup> and Jelena Kovačević<sup>2,4</sup>

<sup>1</sup>Universidad de Concepción, Concepción, Chile

<sup>2</sup>Department of Electrical and Computer Engineering, Carnegie Mellon University, Pittsburgh, PA 15213, USA

<sup>3</sup>Department of Civil and Environmental Engineering, Carnegie Mellon University, Pittsburgh, PA 15213, USA

<sup>4</sup>Department of Biomedical Engineering, Carnegie Mellon University, Pittsburgh, PA 15213, USA

<sup>5</sup>Department of Civil and Environmental Engineering, University of Pittsburgh, PA 15261, USA

(Received May 18, 2012, Revised February 16, 2013, Accepted August 22, 2013)

**Abstract.** An indirect approach is explored for structural health bridge monitoring allowing for wide, yet cost-effective, bridge stock coverage. The detection capability of the approach is tested in a laboratory setting for three different reversible proxy types of damage scenarios: changes in the support conditions (rotational restraint), additional damping, and an added mass at the midspan. A set of frequency features is used in conjunction with a support vector machine classifier on data measured from a passing vehicle at the wheel and suspension levels, and directly from the bridge structure for comparison. For each type of damage, four levels of severity were explored. The results show that for each damage type, the classification accuracy based on data measured from the passing vehicle is, on average, as good as or better than the classification accuracy based on data measured from the bridge. Classification accuracy showed a steady trend for low (1-1.75 m/s) and high vehicle speeds (2-2.75 m/s), with a decrease of about 7% for the latter. These results show promise towards a highly mobile structural health bridge monitoring system for wide and cost-effective bridge stock coverage.

**Keywords:** indirect SHM; laboratory experiment; damage detection; classification

---

### 1. Introduction

The importance and need for bridge inspection and monitoring has increasingly become more apparent in the aftermath of catastrophic collapses, such as those that have occurred recently around the world (I-35W bridge over Mississippi River, USA, Aug 1 2007; Shershah Bridge, Pakistan, Sep 1 2007; Harp Road bridge, USA, Aug 15 2007; Loncomilla Bridge, Chile, Nov 18, 2004). In many countries, the assessment of bridges is done at fixed time intervals. For example, in the United States, bridges are visually inspected every two years, and then, if signs of deterioration are visible, more accurate evaluation is conducted using commercially available nondestructive evaluation techniques such as: acoustic emission, electromagnetic testing or liquid penetrant

---

\*Corresponding author, Professor, E-mail: [facerda@udec.cl](mailto:facerda@udec.cl)

testing, among others. In the past two decades, the interest of both researchers and practitioners in structural health monitoring (SHM) methods has escalated. SHM allows for the evolution of the maintenance practice from “time-based” to “condition-based”, which implies that a sensing system, integrated with the structure or the mechanical system, performs periodically-spaced measurements. The statistical analysis of damage-sensitive features extracted from these measurements enables one to determine the current state of system health and to notify in real time when degradation or damage occurs (Doebbling *et al.* 1998, Carden and Fanning 2004, Farrar and Worden 2007). This approach can be referred to as *direct monitoring*. The objective of any direct bridge monitoring system is to establish the state of a bridge in terms of presence, location, severity, and type of damage (Rytter 1993, Farrar and Worden 2007). Owing to the size and the number of functionally obsolete or structurally deficient bridges in the United States alone (FHWA 2011), the price tag for instrumenting all of them is still prohibitive despite recent advances in the area of SHM (e.g., Chang 2011, Frangopol *et al.* 2010, Casciati and Giordano 2010).

In this paper, the hypothesis experimentally investigated is that an array of sensors, mounted on moving vehicles that travel across the bridge of interest, can be helpful in identifying structural damage and thus serve as an indicator for more detailed analysis and evaluation that might include in-depth bridge inspection and specific instrumentation. This approach can be referred to as *indirect health monitoring*. The indirect approach can be used in multiple un-instrumented bridges at a low cost and without the need for on-site maintenance. It may be viewed as complementary and, if needed, as a substitute for a global direct health monitoring approach if proved to be accurate and effective. Thus, this strategy might help fulfill the need for a practical and cost-effective solution for broad coverage of the bridge population, and help mitigate the costs associated with existing direct SHM practices (Farhey 2005, 2007, Frangopol *et al.* 2008).

The idea of indirect SHM is not new. It was first formulated by Yang (2004, 2005) who modeled the interaction of a sprung mass traveling on an Euler-Bernoulli beam to extract the beam’s fundamental natural frequency. The model was validated experimentally using an instrumented two-wheeled cart attached to a vehicle traveling over a simply supported girder bridge (Lin and Yang 2005). A number of additional studies have been conducted since. In each case, the goal was to detect damage, develop more accurate techniques using limited data for identifying dynamic parameters such as the natural frequencies of the bridge and damping, and to validate these techniques by applying them to increasingly more realistic situations. Some of these efforts are reviewed in what follows.

Yang and Chang (2009) report results associated with field experiments where the first two natural frequencies of a bridge are extracted from the vehicle response by using empirical mode decomposition. Bu *et al.* (2006) develop a damage identification scheme based on optimizing a damage parameter vector. The dynamic response of a vehicle moving on top of a simply supported Euler–Bernoulli beam is simulated by a mathematical model. The damage is defined in terms of the reduction of flexural stiffness. The model incorporates noise measurements, road surface roughness, and errors such as underestimating vehicle parameters or bridge flexural stiffness.

Kim and Kawatani (2008) develop a pseudo-static damage detection method that makes use of the coupled vibration of a vehicle-bridge system. The method requires data collected from both the bridge and the vehicle to characterize the damage. A numerical model that includes the roadway roughness effect is used to test the approach. The pseudo-static approach is subsequently validated experimentally for different vehicle speeds and different reduction amounts of girder’s moment of inertia (Kim *et al.* 2010). McGetrick *et al.* (2009) model a simplified quarter car-bridge interaction to extract the fundamental natural frequency and corresponding damping of the bridge from the

spectra of the vehicle accelerations. They found that better accuracy is achieved at lower speeds and smoother road profiles. Moreover, the magnitudes of the acceleration power spectral density's peaks decrease with increasing bridge damping. This decrease is easier to detect with a smoother road profile. This work is validated experimentally by observing the effects of a vehicle moving across a steel girder that included a road surface profile, different vehicle mass and speeds (McGetrick *et al.* 2010).

Isemoto *et al.* (2010) develop a hypothesis-testing scheme for damage detection based on the vehicle vertical acceleration data. An experimental vehicle-bridge model including roadway roughness, is used. However, only severe damage scenarios were identified. Miyamoto and Yabe (2011) exploit the vibration induced by a public bus for the indirect health monitoring of existing short- and medium-span reinforced/prestressed concrete bridges. The tests show a correlation between the vehicle vertical acceleration and the bridge vibration at midspan. Using a numerical 3D finite element model, they find the distribution of characteristic deflection for a particular driving speed and two severe damage scenarios.

Yin and Tang (2011) use the vertical displacement from the vehicle to identify tension loss and deck damage from numerical models. The relative displacement of a passing vehicle of a bridge with known damaged conditions is used to generate a vector basis. A proper orthogonal decomposition of the relative displacement of a vehicle passing a bridge with an unknown damage condition is optimized with a known basis, and parameters of the unknown damaged bridges are reconstructed. Sirigoringo and Fujino (2012) estimate the fundamental natural frequency of a bridge using the response of a passing instrumented vehicle. They conduct full-scale experiments on a simply supported short-span bridge by using a light commercial vehicle. The frequency spectra from the vehicle's dynamic responses reveal the first natural frequency of the bridge. The experimental study considered traveling speed ranging from 10 to 30 m/s. More recently, González *et al.* (2012) proposed a methodology to identify the damping of a bridge from the vehicle response.

The initial results of an ongoing study are shown here. This work aims at bridging the gap from parameter identification to bridge health monitoring in an indirect fashion. A laboratory bridge model subjected to different vehicle speeds, two different types of reversible damage scenarios, and reversible changes of structural boundary conditions is used. In addition to the indirect measurement of the bridge motion obtained through the vehicle vibration, three sensors are installed directly on the bridge. Contrary to previous studies, the indirect and the direct data are used independently, and a new detection algorithm is introduced. This experimental setup allows for the comparison of the indirect and the direct strategies and evaluation of the effectiveness of the indirect damage detection algorithm.

The authors acknowledge that implementing the indirect monitoring approach assumes as the "ground truth" that the bridge is in an original sound condition. The baseline for the indirect monitoring approach is taken from the response of the vehicle; therefore, there is no need to instrument the bridge. At this early research stage, only data from a specific pristine bridge is collected as the baseline and classified against data collected when the same bridge is modified.

## 2. Experimental setup and protocol

A laboratory experimental setup is built to collect data from a vehicle, which could be used to detect changes in the condition of the bridge. Using this model, acceleration data from a bridge

structure and a vehicle passing over it is collected and later analyzed for characterizing vehicle-bridge interaction patterns. The complete experimental setup consists of mechanical structural components that make up the bridge and vehicle system, a vehicle motion control system, and data acquisition equipment. The different mechanical components resemble a simply supported bridge structure and a four-wheeled vehicle with an independent suspension system at each wheel. The motion control equipment is able to move the vehicle over an acceleration ramp, the simply supported bridge and deceleration ramp. Through this path, the vehicle accelerates until it reaches a target speed before the end of the acceleration ramp, and then maintains a constant speed over the bridge, followed by a deceleration of the vehicle so that it stops at the end of the deceleration ramp. The data acquisition system records accelerations at different locations on the vehicle and the bridge, as well as the position of the vehicle. This experimental setup is inspired by the work of Kim *et al.* (2010).

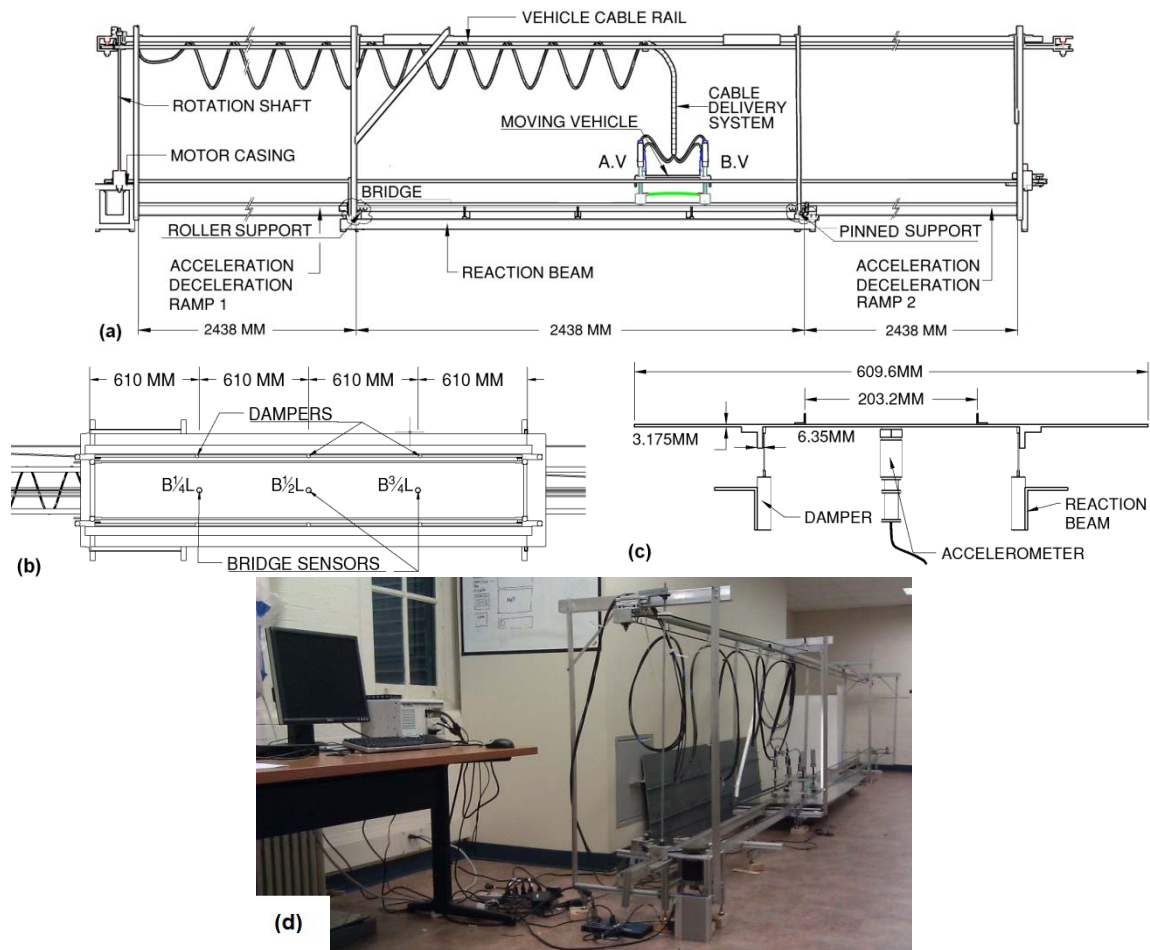


Fig. 1 Experimental setup: (a) Elevation of setup, (b) Bridge bottom view and (c) Bridge cross section (d) Setup overview picture

An overview of the setup is shown in Fig. 1. The vehicle, approximately in the middle of Fig. 1(a), is pulled by a belt system. The belt is a neoprene belt, 1/4" width. The travelling path of the vehicle corresponds to the acceleration/deceleration ramps and the bridge as labeled in Fig. 1(a). The simply supported bridge structure is in the middle of the travelling path. Below the simply bridge there are two "reaction beams" that are connected to the bridge end supports and used to support added dampers.

The vehicle is instrumented with Vibra-metrics accelerometers (Model 5102) powered by cables supported by a cable delivery system that moves parallel to the vehicle. The cables and the vehicle are propelled by a motor at the leftmost part of the experimental setup.

### 2.1 Details of the bridge and vehicle models

The bridge is simply supported by a roller support at the left and a pinned support at the right. The vehicle enters the bridge from the left. The whole system is constructed to act as a closed force loop system. The longitudinal forces generated by the motor to move the vehicle are transmitted between the two supports by two connecting beams labeled as "reaction beams" in Fig. 1(a). The bridge structure is instrumented with three 5102 Vibra-metrics accelerometers as in Fig. 1(b). The sensors are equally spaced along the longitudinal direction of the bridge and named accordingly as B1/4L, B1/2L and B3/4L where  $L=2438$  mm. The reaction beams act as a support for localized dampers that connect to the bridge structure as in Fig. 1(c). The bridge deck consists of an aluminum plate, and two angle beams act as the bridge girders. On top of the plate, two angle beams serve as rails for the travel path of the vehicle. Detailed dimensions of the bridge section are shown in Fig. 1(c) and a picture of the whole setup is shown in Fig. 1(d).

The bridge has a total weight of 18.3 kg, a fundamental natural frequency of 7.23 Hz, and fraction of critical damping of 3.6%. The corresponding aluminum modulus of elasticity and identified section second moment of area are  $E=6.9 \times 10^{10}$  N/m<sup>2</sup> and  $I \approx 8.15 \times 10^{-8}$  m<sup>4</sup> respectively. These are the properties of the bridge in the pristine condition, later referred to as Scenario 1. The bridge and vehicle models do not resemble a particular full-scale structure. They are treated as a vehicle/bridge system in itself. However, the dimensions follow an approximate scaling factor of  $S=8$  to those of a real structure. Following the scaling laws for elastic vibration analysis, this is proxy for a 2.6 Hz simply supported girder structure. The speed has a scaling factor of  $S^{1/2}$ .

Fig. 2(a) shows a 3D view of the vehicle constructed for the experimental setup with the main components labeled. The vehicle is instrumented with two accelerometers connected to the suspension shafts in order to record the acceleration at the wheel level and two accelerometers placed on the suspension to acquire data filtered by the suspension system. To keep the symmetry of the vehicle, two calibrated weights are placed on top of the un-sensed wheel shafts. Similarly to the bridge structure, the vehicle is built mainly with aluminum parts.

Two reference points are labeled on the longitudinal direction of the vehicle as points A Vehicle (A.V) and B Vehicle (B.V). A top view of the vehicle is shown in Fig. 2(b). The length and width of the vehicle as well as the labels assigned to each of the four sensors are also indicated. The sensor labels are defined by their position and location to the reference point. Suspension A.V and Suspension B.V are labeled S.A.V and S.B.V respectively, and the two wheel level sensor locations are labeled W.A.V and W.B.V. A picture of the model vehicle is shown in Fig. 2(c).

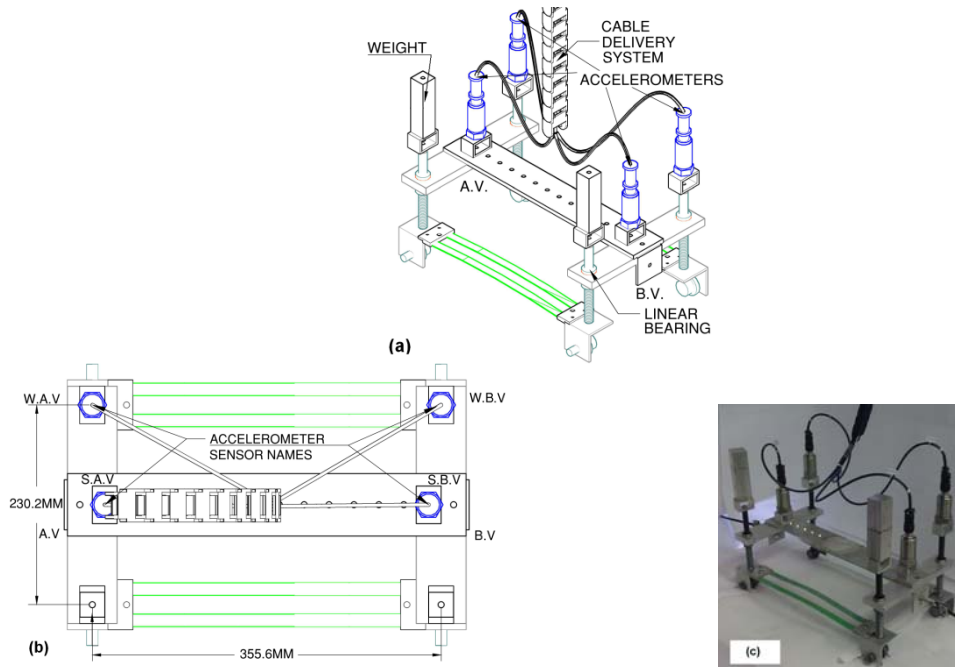


Fig. 2 Experimental vehicle CAD drawings: (a) 3D view, (b) Top view and (c) Vehicle picture

Table 1 Vehicle properties

Vehicle weight [kg]	4.8
A.V axle frequency [Hz]	5.0
B.V axle frequency [Hz]	5.5

The frequency of the A.V and B.V axles of the vehicle are examined through free vibration experiments on the suspension. As the vehicle moves along the traveling path, the lengths of the belts at both sides of the vehicle vary. This variation affects the vehicle's dynamics as a whole vehicle-belt system. Free vibration experiments are performed on the vehicle-belt system with the vehicle at different locations. A frequency of about 6 Hz can be identified for both axles by averaging the frequency power spectrum obtained from five free vibration signals. However, depending on the location of the vehicle, other frequencies are also present in the system. The varying frequencies introduced by the belt can be regarded as system noise and make the damage classification task more difficult; good results in such conditions make therefore a stronger point for the classification results shown later in this paper.

Another set of free-vibration experiments with the belt disconnected from the vehicle are run for both axles. The vehicle frequencies are summarized in Table 1. Damping in both axles is observed to be similar to the critical damping; that is, at the limit between vibration and non-vibration. The vehicle/bridge mass ratio of the model is about 25%, which is higher than what would be expected in a full-scale scenario.

## 2.2 Motion control and data acquisition equipment

A National Instruments® PXI system running in LabView® is assembled to operate the instrumented vehicle and to allow for data acquisition and storage. The system consists of a PXI Chassis (NI PXI 1031) with a motion control card (NI PXI 7342), a motion interface (UMI 7772), a stepper drive (P70360) and a dual shaft stepper motor (NEMA 34). A feedback loop for position is achieved with an encoder. The acceleration data are digitized and stored for post-processing using two digitizers (NI 9234) in an NI CompactDAQ module. Both digitizers feed the data into the same data file. The effective sampling rate is about 1650 Hz, the minimum for the equipment.

A physical mark is made at the beginning and at the end of the travelling path of the vehicle to produce an acceleration spike that is used to align all the acceleration runs of a specific scenario.

## 2.3 Protocol

Three different types of “damage” scenarios are designed: (1) variations on the support condition by imposing rotational restraints, 2) increase of damping at different locations, and (3) a mass increase at the midspan. For each type, four levels of severity are devised in order to obtain a total of 12 different damage scenarios. Table 2 shows the twelve conditions of damage. For each case the fundamental resonance frequency and the corresponding critical damping are reported and compared to the baseline, i.e., Scenario 1. For all cases, the fundamental natural frequency of vibration and the damping coefficient are determined by means of conventional free-vibration experiments.

The rotational restraint mechanism is built into each of the four beam supports of the bridge model. As shown in Fig. 3(a), an aluminum bar is attached to the main girder of the bridge at one extreme and connected to the support at the other extreme to provide vertical restraint. The plate is drilled down to 6.35 mm with 12.7 mm radius to provide only a partial restraint.

Variation of the rotational restraints simulates the case of rubber bearings becoming stiffer in time or steel corrosion occurring on rocker supports (Chajes *et al.* 1997, Kim *et al.* 2009). This condition is a common cause of undesired stress in the structure, and therefore a reduction in the load capacity. In Table 2, the variations of the rotational restraints are described as scenarios SC2 to SC5. In Scenarios 2-5, one, two, three and all four supports are restrained, respectively. As expected, the greater the number of rotational restraints, the higher the fundamental frequency, which provides an indicator of change to the bridge structure.

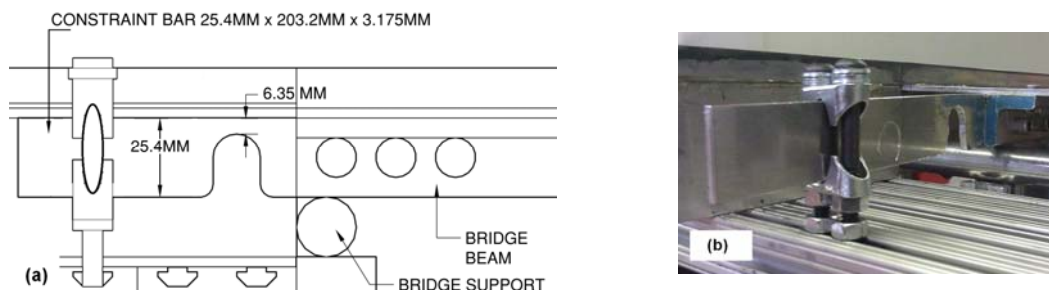


Fig. 3 Detail 1 – Roller support - Rotational restraint (a) technical drawing and (b) picture.

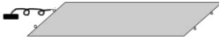
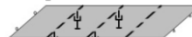
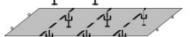
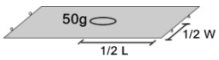
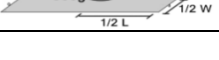
The variation of localized damping is achieved by adding dampers to the bridge at those locations schematized in Table 2 (Scenarios 6 to 9) according to the scheme presented in Fig. 1(c). A set of AIRPOT adjustable dampers is used. The dampers are calibrated to provide a damping coefficient  $c \approx 1.3 \text{ N}\cdot\text{s/m}$ . In Scenarios 6-9, one, two, four and six dampers, respectively are attached to the bridge structure as depicted in the schematics of Table 2.

Finally, the concentrated mass at the midspan of the structure consisted of weights equal to 50 g, 100 g, 200 g and 300 g, and referred to as Scenarios 10 to 13, respectively, in Table 2. As expected, the presence of the mass decreased the fundamental frequency of vibration of the structure.

Eight different vehicle speeds, varying from 1 m/s to 2.75 m/s, are considered for each damage scenario. The speed range of the experiments is close to 10-30 km/hr range in a full-case structure.

Because of the design of the system, when applying additional damping the system does not behave as a single degree of freedom damped system. In Scenarios 06-09 from Table 2 with additional damping, there is a coupling effect between the stiffness of the reaction beams and the bridge structure causing a slight increase in the measured fundamental frequency. This effect is verified with an analytical model.

Table 2 Damage scenarios

Schematics	SC	f [Hz]	% f shift	% $\zeta_{\text{crit}}$	% $\zeta_{\text{crit}}$ shift
	01	7.23	0.00	3.63	0.00
	02	7.46	3.17	6.34	74.9
	03	7.66	6.00	6.45	77.8
	04	8.11	12.2	7.97	120
	05	8.56	18.4	9.37	158
	06	7.24	0.17	8.52	135
	07	7.25	0.28	11.3	212
	08	7.28	0.73	26.4	629
	09	7.30	0.98	31.4	767
	10	7.19	-0.56	4.44	22.5
	11	7.18	-0.66	4.34	19.5
	12	7.14	-1.29	4.07	12.3
	13	7.09	-1.85	4.37	20.5

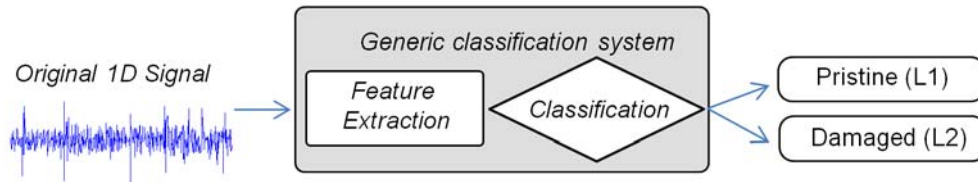


Fig. 4 General classification system

### 3. Signal analysis and classification

The task of distinguishing various bridge conditions is a signal-processing task of classification. The classification process is described first in general, and then is explained how it is used in the classification experiments. Assume a real signal  $x$  of length  $N$ , i.e.,  $X \subset R^N$  (see Original signal in Fig. 4). The problem, then, can be formulated as that of designing a map from the signal space of vibrational signals  $X \subset R^N$  to a response space of class labels  $Y \subset \{1, 2, \dots, C\}$  (in Fig. 4 these are Damaged and Pristine labels). That is, the decision  $d: X \rightarrow Y$  is the map that associates an input signal with a class label.

A general classification system consists of a feature extractor and a classifier (see Fig. 4). Since the dimensionality of the input space is typically large, the feature extractor is introduced to reduce this dimensionality by setting up a feature space  $F \subset R^k$  where  $k \leq N$  between the input space and the response space. The feature extractor is the map defined as  $f: X \rightarrow F$  and the classifier as a map  $g: F \rightarrow Y$ .

#### 3.1 Preprocessing

Fig. 5 shows a signal obtained from the vibration of the vehicle, from the time when it starts moving, through its motion across the bridge, until it has come to a stop. The only relevant information for the bridge characterization, however, is that of the vehicle moving across the bridge. A reference start time is chosen as the moment when the rear wheels enter the bridge and reference end time the moment when the front wheels exit the bridge; that portion of the signal is highlighted in Figs. 5(a)-5(d) by the two vertical lines. The extracted portions of the signals are then normalized to have zero mean and unit variance.

#### 3.2 Feature Extraction

A linear structural system can be characterized in the frequency domain by its predominant natural frequencies, their corresponding mode shapes and damping values. The use of frequency spectra characteristics for damage detection is explored in this work.

The fundamental frequency of the bridge, as shown in Table 2 ranges from 7.2 to 8.6 Hz approximately. The  $n^{\text{th}}$  frequency of a simple supported beam is  $n^2 \cdot f_1$ , where  $f_1$  is the first mode. The second frequency range goes approximately from 28 to 35 Hz. However, this range is reduced because of the presence of the vehicle mass acting on the bridge. Considering the fundamental natural frequencies of the damage scenarios and the vehicle main bouncing frequency, the analysis

is limited arbitrarily to a frequency spectrum of up to 33 Hz allowing for a second bridge mode to influence the response.

For example, looking at Fig. 6 and the spectra (discrete Fourier transform, DFT) of the signals from two different scenarios, a pristine and a damaged one, it can be seen that, potentially, the responses can be told apart from separate sensors by looking at magnitudes of certain characteristic frequencies. Thus, the authors decided to use frequencies as features, hoping to distinguish among different scenarios. The use of additional features might even improve the results shown later in this study. The task is then to find a set of such features to maximize differentiation between classes.

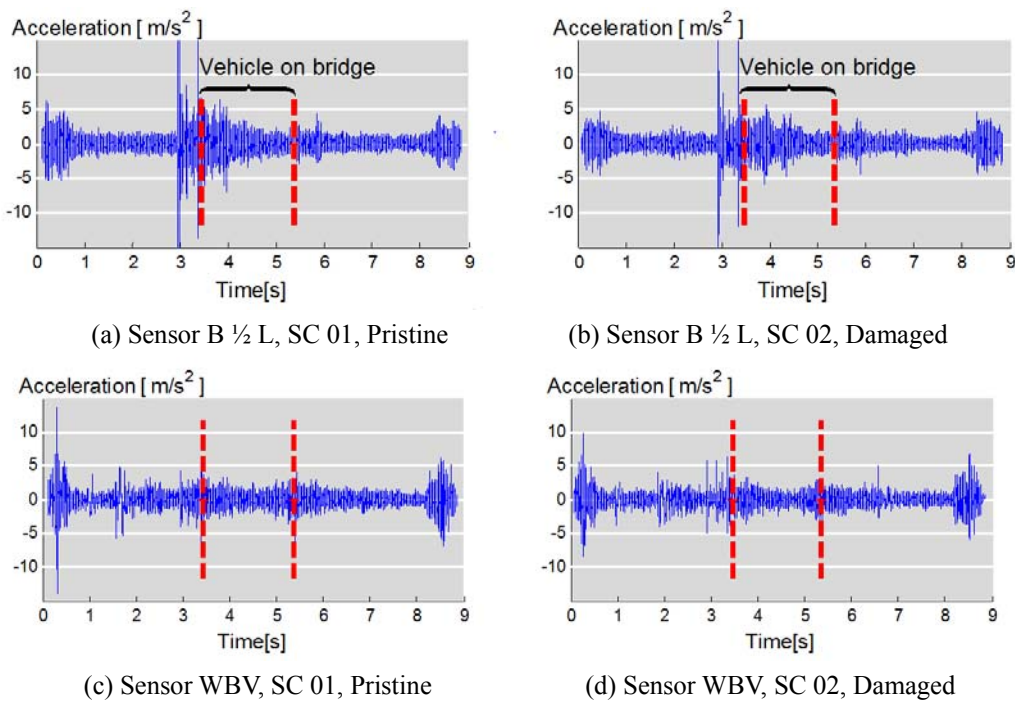


Fig. 5 Time-domain signals

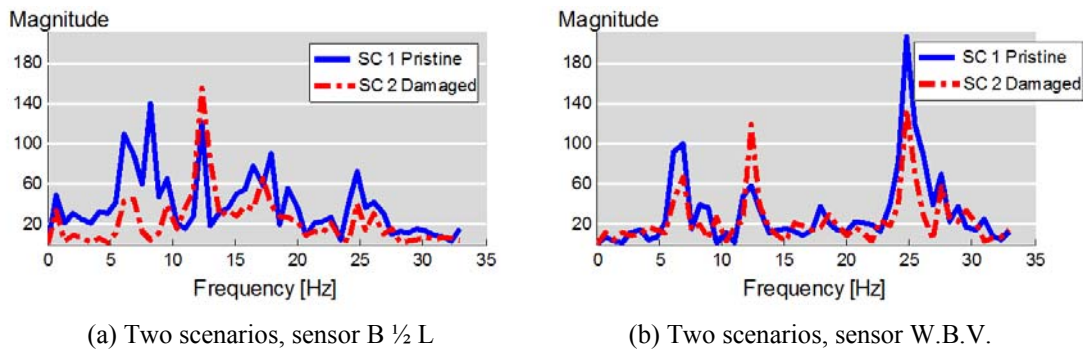


Fig. 6 Discrete Fourier transform of the signal

Since the acceleration signal contains a large number of spikes and other transient signals, the spectra are noisy with little consistency between runs. To reduce noise and keep non-transient frequencies of interest, a typical approach is to average the spectra across frequency. Averaging the frequency spectra is a well-known technique used in noisy signal processing. For example, in radar signal analysis, a redundant number of antennas capture noisy signals from the same source and average them to increase the signal to noise ratio (Keeler and Passarelli 1989).

After averaging, the frequency-domain energy distribution for each scenario is calculated. This technique relies on the assumption that each scenario has its unique energy distribution in the frequency domain. Since the goal is to tell classes apart and not individual runs, all the energy distributions from the same class are averaged. The mean energy distribution is used as the representative member of that class.

Fig. 7 shows the distinctive presence of some frequencies that are neither from the bridge nor the vehicle. For example, the most significant peaks are around 13 Hz and 25 Hz in Fig. 7(b). Considering the nature of the problem, the analyzed signals represent the portion of time where the vehicle is traversing the bridge, therefore, these signals do not represent a single structure, rather, a structure made up of the vehicle-bridge coupled effect with vehicle at different locations along the bridge.

Let  $\{x_i^{(c)}\}_{i=1}^{N_c}$  be a set of signals with  $N_c$  samples belonging to Class  $c$ . The Fourier energy map is

$$\Gamma_c(j) = \frac{\sum_{i=1}^{N_c} \|w_j^T x_i^{(c)}\|^2}{\sum_{i=1}^{N_c} \|x_i^{(c)}\|^2} \tag{1}$$

where  $w$  denotes Fourier basis vector and  $j$  denotes the frequency band. To evaluate the power of discrimination of every Fourier basis vector, we need a discriminant measure  $D$  to evaluate the power of discrimination. The higher discriminant power is assumed to provide higher discrimination between classes.

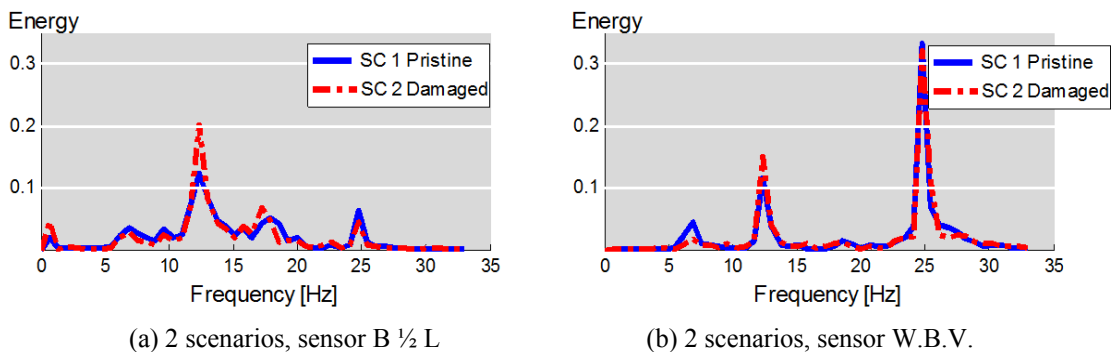


Fig. 7 Mean energy distribution (normalized to unit energy)

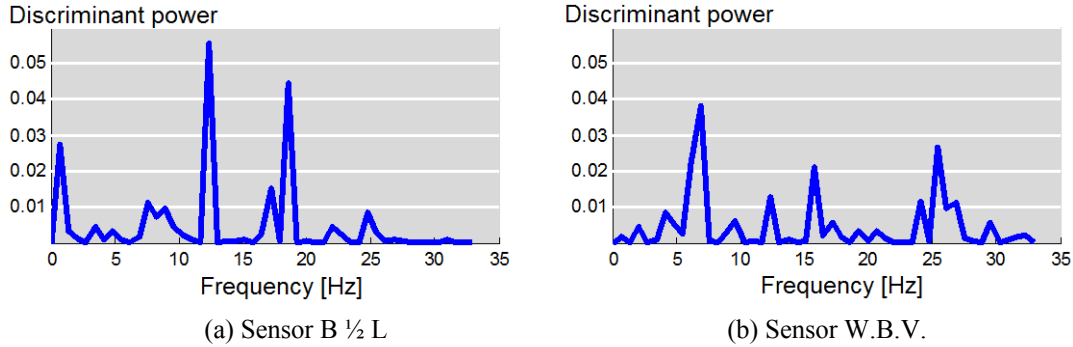


Fig. 8 Discriminant power (normalized to unit discriminant power)

For the  $j$ th Fourier basis vector, the power of discrimination  $\Delta$  is denoted by

$$\Delta_j = D(\{\Gamma_c(j)\}_{c=1}^C) \tag{2}$$

There exist numerous choices for the discriminant measure; the J-divergence was used in this work (Kullback and Leibler 1951) because it is one of the most famous measurements to quantify the difference or discrepancy of probability density functions (PDFs) in information theory. Moreover, by definition it is additive, which helps in multiclass situations. Let  $p = \{p_i\}_{i=1}^n$ ,  $q = \{q_i\}_{i=1}^n$  be two nonnegative sequences with  $\sum p_i = \sum q_i = 1$ , J-divergence between  $p$  and  $q$  is:

$$J(p, q) = \sum_{i=1}^n p_i \log \frac{p_i}{q_i} + \sum_{i=1}^n q_i \log \frac{q_i}{p_i} \tag{3}$$

Fig. 8 shows a graph of the discriminant power between the frequency signals previously depicted in Fig. 7.

To help understand the feature selection method, a summary of the assumptions and conclusions thus far is presented: 1) To differentiate signals from different scenarios, frequencies are used as features. 2) If the discriminant power is higher, it is easier to discriminate between classes. The discriminant power will thus predict how well a feature will perform during classification. 3) A small number of frequencies provide most of the discriminative power; in other words, the frequency feature set is sparse. Just those frequencies that have large discriminative power are selected (this is called nonlinear approximation); see Fig. 9.

This selection method performs nonlinear approximation in the Fourier domain and is data adaptive. Different data may give different frequency information and different discriminant powers. Since this method learns from the data and always chooses the frequencies with large discriminant power, it is more robust than traditional linear approximation.

Fig. 10 shows the feature space of the first three features. Blue circles denote the pristine scenario and red asterisks the damaged scenario. Using just three Fourier discriminant basis vectors, it is easy to separate the two classes.

Algorithm (Fourier Discriminant Basis Vectors Selection)

Task: Find  $k(\leq n)$  most discriminant Fourier basis vectors

Given a dataset consisting of  $C$  classes of signals  $\{\{x_i^{(c)}\}_{i=1}^{N_c}\}_{c=1}^C$

Step 1: Take the DFT of  $x$ .

Step 2: Construct Fourier energy map  $\Gamma_c$  for  $c = 1, \dots, C$

Step 3: Determine the power of discrimination  $\Delta_j = D(\{\Gamma_c(j)\}_{c=1}^C)$  for every Fourier basis vector  $w_j$

Step 4: Order Fourier basis vectors by their power of discrimination.

Step 5: Use  $k(\leq n)$  most discriminant Fourier basis vectors for constructing classifier

Fig. 9 Summary of feature extraction process

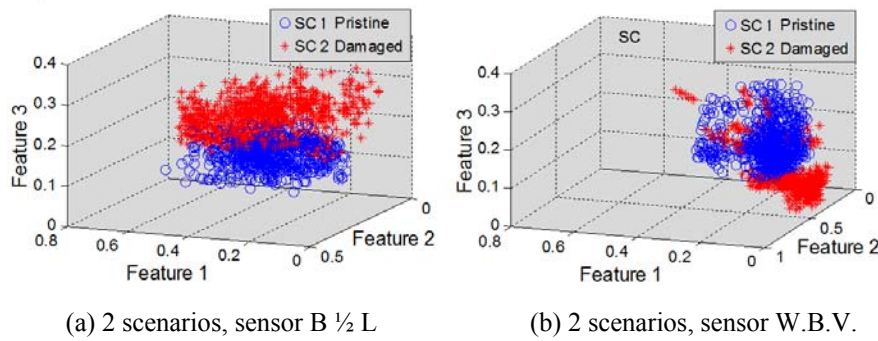


Fig. 10 Clustering of two scenarios

#### 4. Classification

The second part of a classification system is the classifier itself. It takes as input a feature vector and outputs a class label. The classification problem here is called supervised learning, as a labeled training set is given. Many different classifiers are available, such as naïve Bayes, neural networks and many others (Duda *et al.* 2000). In this work, the support vector machine (SVM) classifier is chosen, which is now briefly described.

When looking for the best boundary to separate classes, two things are desired: 1) the boundary should give high classification accuracy; 2) avoid overfitting. To satisfy these two requirements, SVM maximizes the margin, that is, the distance between a decision boundary and a data point, and expresses it as a function of the weight vector and bias of the separating hyperplane, which is used to separate the space in two.

There are 30 samples in each class. If 3 out of 30 samples are randomly chosen and averaged, then there will be 4060 potential different choices (30 choose 3 binomial coefficients). As the study dataset, 1000 out of 4060 samples are randomly chosen for each scenario. A 20-fold cross validation is performed. Each time, 2000 data samples, consisting of 1900 training samples and

100 testing samples, are used to create and test the SVM-based classifier. We then used our Fourier discriminant basis search algorithm and selected the top 5 frequencies that provide the largest discriminant power as features. Then kernel SVM is used as the classifier.

## 5. Results and discussion

The results of the classification experiments are presented and discussed in terms of the classification accuracy, which is defined as the number of test samples correctly classified divided by the total number of test samples.

In the two classes defined, pristine and damaged, scenarios 2-13 belonged to the latter class. The data collected from all seven accelerometers are used.

Fig. 11 shows the variation of the average classification accuracy for different variables. Fig. 11(a) shows the average across the different severities, speeds and sensor locations for each damage type. The three bridge sensors, B1/4L, B1/2L and B3/4L, are averaged and referred to as “Bridge”, the two sensors at the wheel level, (W.A.V and W.B.V) are averaged and referred to as “Wheel” and the two sensors at the suspension level, (S.A.V and S.B.V) are averaged and referred to as “Suspension”. The standard deviation across the averaged variables is shown at the top of each bar. An average classification accuracy for all the sensors for each damage type is depicted with a black line and corresponding percentage. The baseline in Figs. 11(a) and 11(b) is 50%, which is the expected probability of randomly choosing between two labels (pristine or damaged). Classification accuracy values of over 90% are obtained despite the subtle changes introduced in the bridge structure. The amount of change inflicted is deliberately small to test the detection capability of the combined indirect approach using the signal processing techniques described in Section 3. The signals from the sensors located at the wheel level are classified consistently across the different damage types, and more accurately than those from the sensors located on the bridge or on the vehicle at the suspension level.

The classification results in Fig. 11(b) show how the average classification accuracy for all damage scenarios varies for different vehicle speeds. Similarly to Fig. 11(a), each bar represents the mean accuracy classification across the different damage scenarios. At the top of each bar, the corresponding standard deviation is shown. Looking at Fig. 11(b), one can see that there is a jump between the first four speeds, between 1 and 1.75 m/s and the four higher speeds from 2 to 2.75 m/s. The average across the two groups of speeds is shown by a black line and corresponding percentage. There is about a 7% difference in classification accuracy between these two speed ranges. This classification accuracy difference is consistent for the average classification accuracy of the sensors at the different locations (i.e., Bridge, Wheel and Suspension).

Fig. 12 illustrates the sensitivity of the classification method to different levels of severity of the different damage types inflicted in the damage scenarios. Figs. 12(a)-12(c) show the average classification for the different damage severity levels for the rotational restraint damage type for different vehicle speeds. For all of these graphs, the thickness of the line depicts the level of damage. The thinnest line indicates the least amount of damage inflicted (e.g., only one of four rotational restraints imposed in SC2) and the thickest line the maximum amount of damage inflicted (e.g., all four rotational restraints imposed in SC5).

Figs. 12(a)-12(c) show the average classification accuracy for each rotational restraint damage severity level for the signals from all the sensors on the bridge, all the sensors on the suspension, and all the sensors on the wheel, respectively. Figs. 12(d)-12(f) break the results down for each

sensor and show the average classification accuracy for each rotational restraint damage severity level for each signal from the three sensors on the bridge, B1/4L, B1/2L and B3/4L; from the two sensors on the suspension, S.A.V and S.B.V; and from the two sensors on the wheel, W.A.V and W.B.V, respectively.

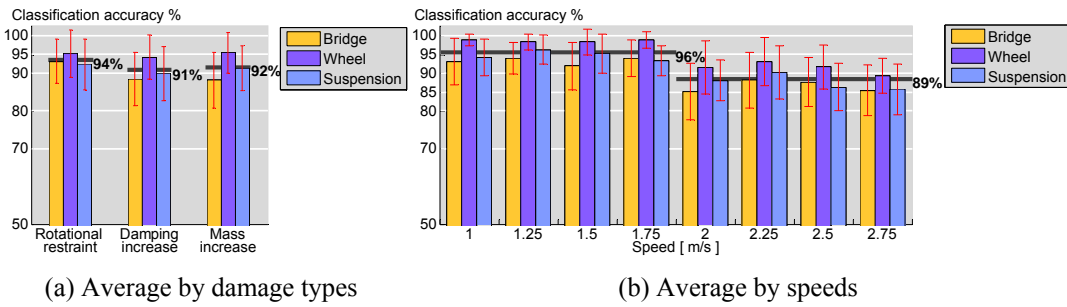


Fig. 11 Classification accuracy results

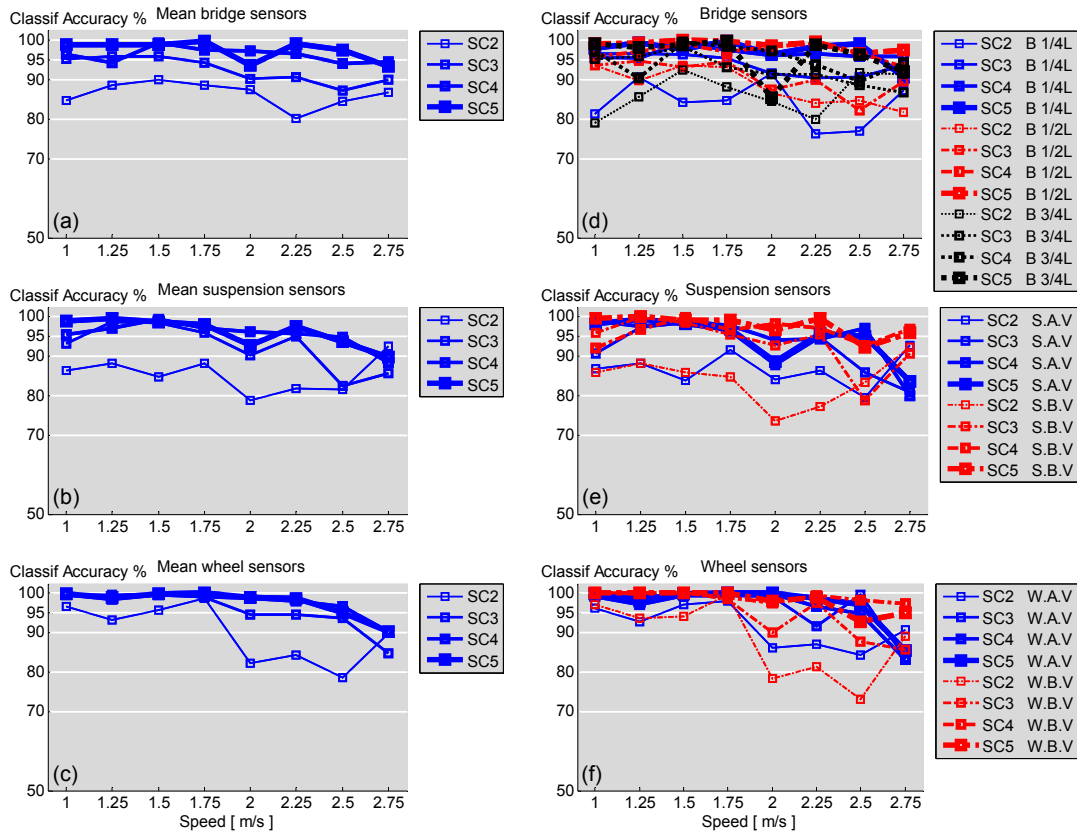


Fig. 12 Classification results for rotational restraint scenarios

Fig. 12 demonstrates that the classification accuracy for SC2 is lower than for the other rotational restraint scenarios (SC3, SC4 and SC5). For SC2, there is a variation in the classification accuracy with respect to speed. However, more severe rotational restraint scenarios seem to be less dependent on speed, with high classification accuracy for low speeds and a slight parabolic decrease for higher speeds. No significant difference in the classification accuracy is apparent in Figs. 12(a)-12(c) regarding the sensor location. This shows that, in terms of classification accuracy, the signal processing approach performs well with sensor data from the vehicle (sensor or wheel) as with sensor data directly measured on the bridge. The wheel sensors perform slightly better than the suspension or bridge sensors. In other words, the results indicate that in this particular set of experiments, and for the signal processing scheme used, the indirect approach has a classification accuracy that is as good as that of the direct approach. Figs. 12(d)-12(f) show that the lowest classification accuracies are those of the least severe damage scenarios. The most severe scenarios are all grouped with high classification accuracies.

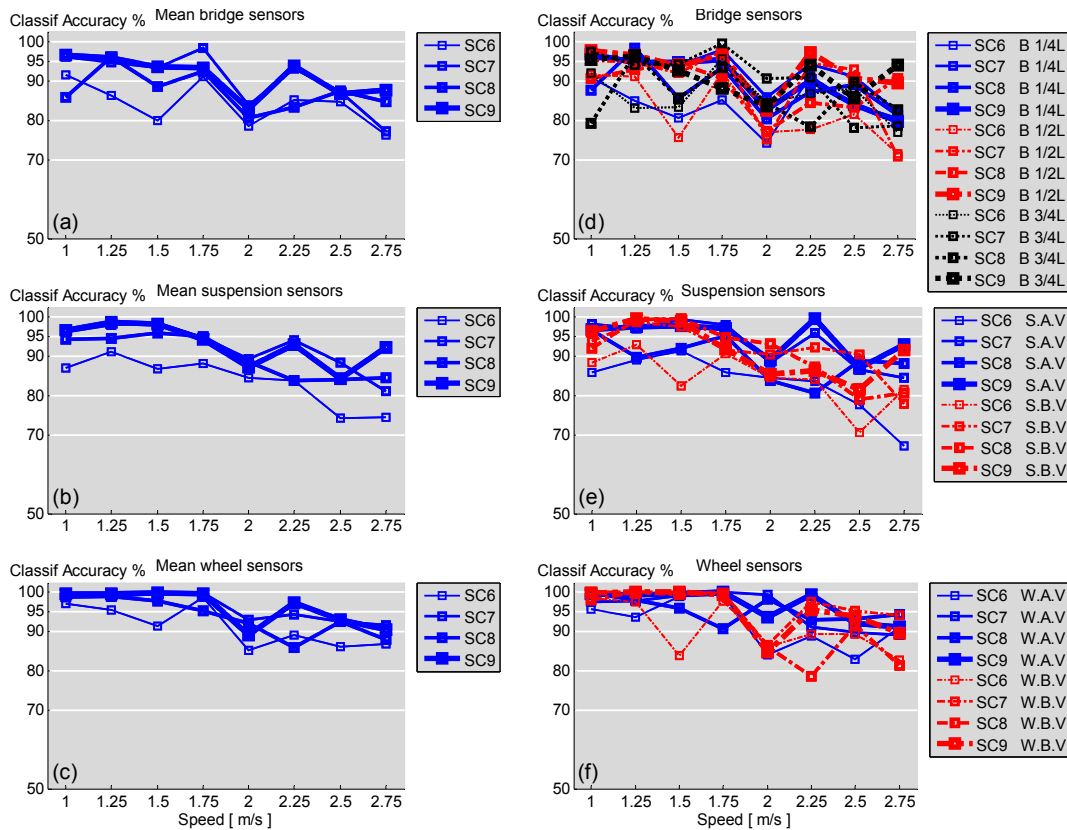


Fig. 13 Classification results for damping increase scenarios

Figs. 13 and 14 are similar in nature to Fig. 12, but display the classification accuracies for the two other damage types explored: the scenarios with increasing amounts of damping and with increasing amounts of mass. Figs. 13(a)-13(c) show Scenario 6, the scenario with the single

damper, as the one with the least classification accuracy across all speeds. In terms of vehicle speed, a decrease in the classification accuracy appears to occur when the vehicle speed is 2 m/s as shown in Fig. 13(a). The same observations from Fig. 12 apply to Fig. 13 as well. There is a slight decrease of the classification accuracy at higher speeds, and the classification accuracy seems to be independent of the sensor location; that is, there is little difference in the classification capability between the direct and the indirect approaches.

Fig. 14 shows the classification results for the scenarios with a mass increase at the midspan. Even though the inflicted change in the bridge structure is quite subtle, the classification accuracy is high, especially at lower speeds. The same observations made for Figs. 12 and 13 are valid for Fig. 14 as well, that is, classification accuracies exhibit small variations with respect to the vehicle speed and the sensor locations.

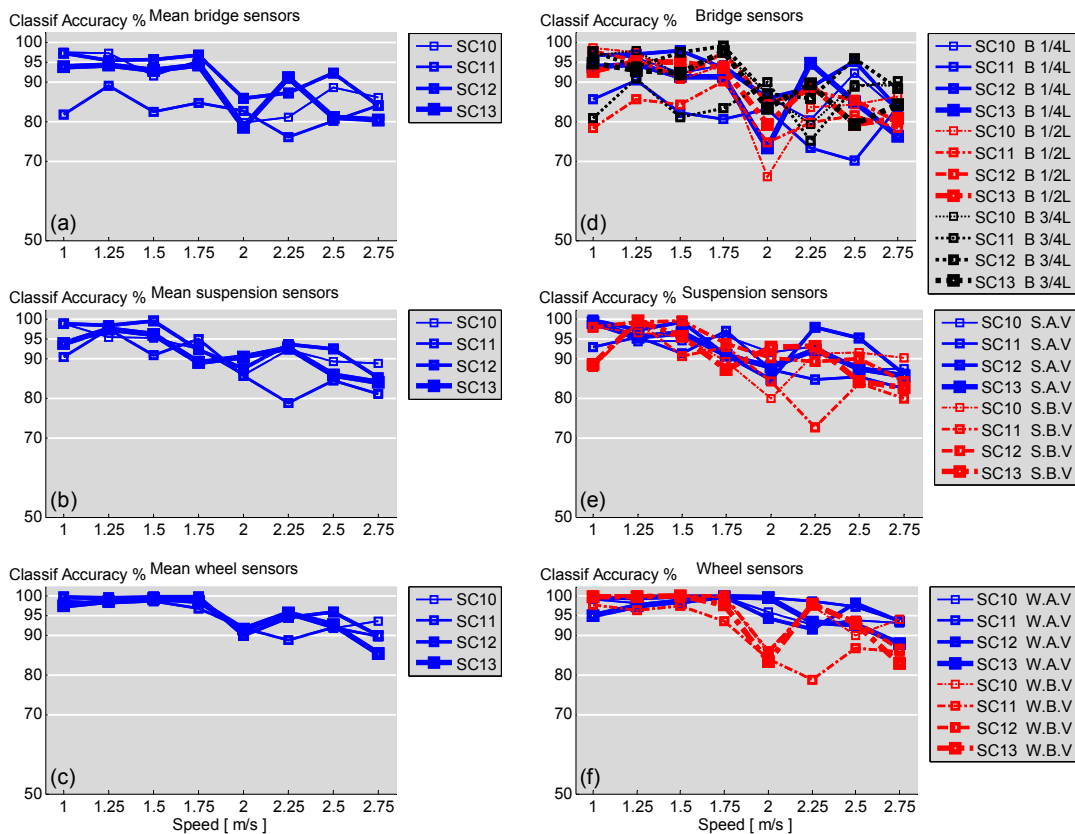


Fig. 14 Classification results for concentrated mass scenarios

## 6. Conclusions

The damage detection capability of an indirect bridge monitoring approach is studied by means of data collected from a moving vehicle and applying signal processing techniques to detect damage of a bridge. The study uses data from a laboratory vehicle-bridge physical model. The

indirect monitoring approach requires no pre-condition on the bridge and is pursued by the authors as an economical and effective bridge SHM approach for a large bridge stock. However, in a full-scale deployment, some bridge parameters such as their geometric configuration and location will be necessary for data pre-processing.

To perform numerous test repetitions, a fully automated vehicle-bridge model needed to be built. In this study, the amount of experimental data samples is significantly greater than that in previous experiments. Each scenario is run 30 times at eight different velocities. Three different reversible damage proxy types were built into the experimental setting, and each damage type had four different severity scenarios.

The synchronized acceleration data from the bridge and the vehicle, and the vehicle position data, allowed for the comparison of the direct and indirect approaches in terms of the accuracy with which each could classify the existence of damage for different extents of damage.

A feature extraction technique based on averaging the power spectrum from a set of data is used to achieve high noise reduction. Then, features extracted from the Fourier domain are automatically chosen from the denoised data samples based on their significance and classified using an SVM classifier. The use of other features and signal processing techniques will be pursued in future research. However, using frequencies and the specific signal processing scheme presented, allowed comparing the direct and indirect monitoring approaches damage detection capability and trends regarding different types of damage, severities of damage and vehicle speeds.

High classification accuracy is achieved across three distinct types of changes inflicted into the bridge structure: 1) a change in the support conditions obtained by introducing rotational restraints at the supports; 2) an increase in the damping of the bridge structure; and 3) a localized mass increase at the midspan of the bridge.

The severity of the changes inflicted on the bridge structure is consistent with higher classification accuracy. For example, SC3, SC4 and SC5 imposed more significant changes into the bridge structure than SC2, and consistently higher classification accuracy is obtained. Nonetheless, the classification accuracy achieved for the subtle change inflicted on SC2 is on average above 85%.

The detection of the various changes in the bridge structure is quite insensitive to the vehicle speed. This effect can be important for practical applications where vehicle speeds cannot be readily controlled. However, a small jump is observed between the lower and higher speeds, where the classification accuracy decreases by about 7% at the higher speeds. At this early research stage, this sudden decrease can only be attributed to the non-linear nature of the dynamic interaction problem.

Independent of the sensor location, high classification accuracy is achieved across all the sensors. The indirect and direct approaches seem to be equally effective for damage detection when applying the proposed signal processing techniques. Of the two sensor locations considered in the indirect approach, the wheel level and the suspension level, the sensors at the wheel level performed better than the sensors at the suspension level.

Given the simplicity of the model considered, the results presented are strictly applicable only to the particular experimental setup and cannot be generalized for full-scale structures at this time. The authors have not yet tested whether the indirect approach can be generalized to different bridge structural configurations and/or with a specific range of dynamic properties. The effect of the vehicle/bridge ratio is not addressed in this work. This parameter will be subject of future investigations. On the other hand, a high degree of consistency is observed in the classification accuracies across the very different types and severity of damage and for different vehicle speeds.

This gives us hope that our approach might be applicable to more general systems.

In reality, data collected about actual damage conditions from the actual structure being monitored will not always be available for use in training. In this case, different detection schemes would have to be used, such as outlier detection, which would help to trigger more in-depth inspection. In the long run, numerical and experimental models that proxy real case scenarios would allow learning the evolution of damage sensitive features obtained either in the direct or indirect fashion from different damaged scenarios. The early detection of those features will allow making more accurate diagnostics and prognosis about the overall structural health.

Clearly, further research is needed to validate the robustness of these results for more realistic systems and conditions, including different roadway roughness profiles, atmospheric conditions and other bridge interaction variables such as different vehicle/bridge mass ratios, the effect of ongoing traffic and torsional effects on the bridge by non-symmetric loading from the vehicle path.

## Acknowledgements

We gratefully acknowledge the support from the National Science Foundation (Award No. CMMI1130616); the Traffic 21 initiative and the T-SET University Transportation Center sponsored by the US Department of Transportation under Grant No. DTRT12-G-UTC11 at Carnegie Mellon University; and the Fulbright-MECESUP Fellowship awarded to the corresponding author. We thank Eduard Romero, Ranny Zhao, Zhe Zhuang and Timothy Pianka, who participated in the construction of the experimental setup and running the experiments. We also thank Michael McCann for his input in the signal processing section.

## References

- Bu, J.Q., Law, S.S. and Zhu, X.Q. (2006), "Innovative bridge condition assessment from dynamic response of a passing vehicle", *J. Eng. Mech - ASCE*, **132**(12), 1372-1379.
- Carden, E.P. and Fanning, P. (2004), "Vibration based condition monitoring: a review", *Struct. Health Monit.*, **3**(4), 355-377.
- Casciati, F. and Giordano, M. (2010), "Structural Health Monitoring", *Proceedings of the 5th European Workshop on Structural Health Monitoring Held at Sorrento*, Naples, Italy, June 28-july 4, DEStech Publications, Inc.
- Chang, F.K. (2011), "Structural Health Monitoring", *Proceedings of the Condition-Based Maintenance and Intelligent Structures*, DEStech Publications.
- Chajes, J., Mertz, D. and Commander, B. (1997), "Experimental load rating of a posted bridge", *J. Bridge Eng.*, **2**(1), 1-10.
- Doebling, S.W., Farrar, Ch.R. and Prime, M.B. (1998), "A summary review of Vibration-based Damage Identification Methods", *Shock Vib.Digest*, **30**, 91-105.
- Duda, R.O., Hart, P.E. and Stork, D.G. (2000), *Pattern classification* (2nd Ed.), Wiley-Interscience.
- Farhey, D.N. (2005), "Bridge instrumentation and monitoring for structural diagnostics", *Struct Health Monit.*, **4**(4), 301-318.
- Farhey, D.N. (2007), "Quantitative assessment and forecast for structurally deficient bridge diagnostics", *Struct Health Monit.*, **6**(1), 39-48.
- Farrar, C.R. and Worden, K. (2007), "An introduction to structural health monitoring", *Philos. T. R. Soc. A*, **365**(1851), 303-315.
- FHWA (2011), Deficient bridges by state and highway system", <http://www.fhwa.dot.gov/bridge/>

- deficient.cfm.
- Frangopol, D.M., Strauss, A. and Kim, S. (2008), "Bridge reliability assessment based on monitoring", *J. Bridge Eng.*, **13**(3), 258-270.
- Frangopol, D.M., Sause, R. and Kusko, Ch. (Eds.) (2010), "Bridge Maintenance, Safety and Management - IABMAS'10", *Proceedings of the 5th International IABMAS Conference*, Philadelphia, USA, 11-15 July, 1st ed. CRC Press.
- González, A., OBrien, E.J. and McGetrick, P.J. (2012), "Identification of damping in a bridge using a moving instrumented vehicle", *J. Sound Vib.*, **331**(18), 4115-4131.
- Isemoto, R., Kim, C.W. and Sugiura, K. (2010), "Abnormal diagnosis of bridges using traffic-induced vibration measurements", *Proceedings of the 23th KKCNN Symposium on Civil Engineering*, Taipei, Taiwan.
- Keeler, R.J. and Passarelli, R.E. (1989), *Signal processing for atmospheric radars*, NCAR/TN-331+STR NCAR TECHNICAL NOTE.
- Kim, C.W. and Kawatani, M. (2008), "Pseudo-static approach for damage identification of bridges based on coupling vibration with a moving vehicle", *Struct. Infrastruct. E.*, **4**(5), 371-379.
- Kim, C.W., Kawatani, M. and Fujimoto, T. (2010), "Identifying bending stiffness change of a beam under a moving vehicle", In *Bridge Maintenance, Safety and Management - IABMAS'10*, 180-180, Bridge Maintenance, Safety and Management. CRC Press.
- Kim, Y.J., Tanovic, R. and Wight, R.G. (2009), "Recent advances in performance evaluation and flexural response of existing bridges", *J. Perform. Constr. Fac.*, **23**(3), 190-200.
- Kullback, S, and Leibler, R.A. (1951), "On Information and Sufficiency", *Ann. Math. Statist* , **22**, 79-86.
- Lin, C.W. and Yang, Y.B. (2005), "Use of a passing vehicle to scan the fundamental bridge frequencies: an experimental verification", *Eng. Struct.*, **27**(13), 1865-1878.
- McGetrick, P.J., González, A. and O'Brien, E.J. (2009), "Theoretical investigation of the use of a moving vehicle to identify bridge dynamic parameters", *Insight: Non-Destructive Testing and Condition Monitoring* , **51**(8), 433-438.
- McGetrick, P.J., Kim, C.W. and O'Brien, E.J. (2010), "Experimental investigation of the detection of bridge dynamic parameters using a moving vehicle", *Proceedings of the 23th KKCNN Symposium on Civil Engineering*, Taipei, Taiwan.
- Miyamoto, A., and Yabe, A. (2011). "Bridge condition assessment based on vibration responses of passenger vehicle", *J. Phys. Conf. Ser.*, **305**(1), doi:10.1088/1742-6596/305/1/012103.
- Rytter, A. (1993), *Vibration based inspection of civil engineering structures*, Ph.D. Dissertation, Department of Building Technology and Structural Engineering, Aalborg University, Denmark.
- Siringoringo, D.M. and Fujino, Y. (2012), "Estimating bridge fundamental frequency from vibration response of instrumented passing vehicle: analytical and experimental study", *Adv. Struct. Eng.*, **15**(3), 417-433.
- Yang, Y.B. and Chang, K.C. (2009), "Extraction of bridge frequencies from the dynamic response of a passing vehicle enhanced by the EMD technique", *J. Sound Vib.*, **322**(4-5), 718-739.
- Yang, Y.B., Lin, C.W. and Yau, J.D. (2004), "Extracting bridge frequencies from the dynamic response of a passing vehicle", *J. Sound Vib.*, **272**(3-5), 471-493.
- Yang, Y.B. and Lin, C.W. (2005), "Vehicle-bridge interaction dynamics and potential applications", *J. Sound Vib.*, **284**(1-2), 205-226.
- Yin, S.H, and Tang, C.Y. (2011), "Identifying cable tension loss and deck damage in a cable-stayed bridge using a moving vehicle", *J. Vib. Acoust.*, **133**(2), 021007.